



Isothermal, Kinetic, and Thermodynamic Studies on the Adsorption of Molybdenum by a Nanostructured Magnetic Material

Elnaz Shargh¹, Hossein Sid Kalal^{2*}, Zahra Shiri-Yekta², Seyed Ebrahim Mousavi³, Mohammad Reza Almasian², Mohammad Tagiof², Hassan Hoveidi¹

¹Department of Environmental Management, Faculty of the Environment, University of Tehran, Tehran, Iran

²Nuclear Fuel Research School, Nuclear Science and Technology Research Institute, AEOI, P.O. Box 11365-3486, Tehran, Iran

³School of Chemical Engineering, College of Engineering, University of Tehran, Tehran, Iran

*Correspondence to

Hossein Sid Kalal,
P.O. Box 11365-3486,
Email: hsidkalal@aeoi.org.ir

Published online December 31, 2020

Abstract

In this study, the magnetic 3-(trimethoxysilyl) propyl methacrylate (TMSPMA) – poly (4-vinylpyridine) (P4VP) was synthesized and characterized. Removal of Molybdenum (Mo) from aqueous solutions using prepared material as nanosorbent was investigated. The magnetic P4VP was prepared by copolymerization of P4VP with TMSPMA. The prepared adsorbent was characterized by various techniques including the X-ray powder diffraction (XRD), scanning electron microscopy (SEM), and Fourier-transform infrared spectroscopy (FTIR). The batch adsorption technique was applied and the effect of several important parameters such as pH of the aqueous solution, adsorbent dose, initial Mo(VI) concentration, contact time, and temperature was evaluated. Desorption behavior of Mo(VI) and the effect of foreign ions (Cd²⁺, Ca²⁺, Co²⁺, Fe³⁺, Ba²⁺ and Pt⁴⁺) in real samples were also investigated. Co (II) and Pt (IV) had a greater impact on the adsorption process than other foreign ions. The maximum capacity for Mo(VI) adsorption on the prepared adsorbent was 4.87 mg/g, which was obtained at a temperature of 40°C with an initial concentration of 10 mg/L of Mo(VI). The adsorption isotherms were best fitted with the Weber Van Vliet isotherm model. The kinetic data were fitted well with the pseudo-second-order equation with a high correlation coefficient ($R^2 > 0.99$). Based on the negative standard Gibbs free energy change ($\Delta G^\circ < 0$) and the positive standard enthalpy change ($\Delta H^\circ > 0$), it was found that the adsorption was an endothermic and a spontaneous process in nature.

Keywords: Molybdenum removal, Batch adsorption, 3-(trimethoxysilyl) propyl methacrylate, Poly (4-vinylpyridine), Magnetic nanosorbent

Received December 3, 2020; Revised December 10, 2020; Accepted December 22, 2020



1. Introduction

Molybdenum (Mo) has important applications for different fields. Mo can be used as an alloying agent in cast iron, steels, reactor vessels, and special batteries due to its various properties. Mo is also applied in solid lubricants, automotive industry, plastics and rubber industry, aircraft engines, glass industry, pigments (for paints, coatings and inks), as well as in electronics industry. There are high concentrations (>5 ppm) of molybdate (MoO₄²⁻) in the environment, which have harmful effects on humans, vegetables, and Animals (1). An examination of the environmental hazards of Mo showed that it is generally a hazardous substance and if swallowed, it can cause severe poisoning. Symptoms of acute poisoning include severe irritation of the gastrointestinal tract with diarrhea, coma, and death from heart failure. It affects the nervous and pulmonary systems in much the same way as it affects the respiratory tract, and it can also cause skin allergies and

severe damage to the eyes. This element is flammable in powder form (2). Mo is the most concentrated trace metal in seawater due to its high stability and weak adsorption. Given the above-mentioned reasons, the separation of Mo is mandatory. Molybdenum-99 (⁹⁹Mo) is a radionuclide used in the nuclear fields and medical practices (2-4). Mo belongs to the fission products and is contained in significant concentrations in highly radioactive waste. Due to the complex chemical properties of Mo, soluble and insoluble complexes are formed. In particular, several problems occur in the concentration, storage, and solidification of high-quality waste (5). The proposed methods for removing molybdate (molybdate includes Mo(VI) ion) from aqueous solutions have been described with various adsorbents, namely carbon cloths (6,7), aluminum oxides (8), pyrite (9,10), natrolite (11), goethite (9), and iron oxide gel (12). Nanomaterials are kinds of materials that have a particle size of 100 nm or

less with particular specifications (13). Many researchers have reported the application of different nanosized adsorbents such as nanoparticles (NPs) and nanotubes (14). Recently, the preparation of magnetic nanoparticles (MNPs) has received a lot of attention because of its various technological applications in water purification, photocatalysis and other separation processes (such as extraction bioseparation (15-17), and separation of different ions (17-32). The MNPs are effective adsorbents due to their large specific surface area, low toxicity, and superparamagnetic behavior. Due to their magnetic properties, they can be used for effective separation in a short time using an external magnetic field (33). Chemical modification and surface functionalization of adsorbents make it possible to use them in various physical, chemical, and biological conditions (34). The Fe_3O_4 MNPs have received a great deal of attention in various academic and technological applications because of their inherent properties (35-37). The present study aimed to synthesize the magnetic poly (4-vinylpyridine) (P4VP), which was prepared by copolymerization of P4VP with 3-(trimethoxysilyl) propyl methacrylate (TMSPMA). The physical and chemical characteristics of the synthesized adsorbent were specified. The adsorbent efficiency in removing Mo(VI) ions from aqueous solutions was investigated. Several important parameters were evaluated and optimized. The kinetic, isotherm, thermodynamic, and error investigations were also performed.

2. Materials and Methods

Sodium molybdate dihydrate ($\text{Na}_2\text{MoO}_4 \cdot 2\text{H}_2\text{O}$) was prepared by diluting a 1000 mg/L Mo(VI) solution. All chemicals and reagents applied in this study were purchased from Merck Company (Merck, Darmstadt, Germany) and met the analytical standard. All solutions were prepared with deionized and double-distilled water. The prepared adsorbent was characterized by several techniques including Fourier-transform infrared spectroscopy (FTIR) (Shimadzo, FT-IR4300 spectrophotometer in the range of 400-4000 cm^{-1}), X-ray powder diffraction (X'pert, Philips, Holland in the 2θ range of 5-100°), and scanning electron microscopy (SEM) (Hitachi S-4160 scanning electron microscope). The concentration of metal ions was determined by inductively coupled plasma (ICP) (Varian liberty 150 XL).

2.1. Synthesis and Functionalization of Fe_3O_4 NPs

First step: $\text{FeCl}_2 \cdot 4\text{H}_2\text{O}$ (3.32 g, 0.05 mmol) and $\text{FeCl}_3 \cdot 6\text{H}_2\text{O}$ (5.4 g, 0.06 mmol) were added to a water solution (80 mL). Ammonia solution (25 wt %) was added to the mixture to adjust the pH value to 9. The resultant mixture was kept at room temperature for 12 hours. Then the NPs were disconnected from the solution with a permanent magnetic, and washed several times with water until the pH value reached 7. Finally, the Fe_3O_4 NPs were dried in a vacuum oven at 80°C for 24 hours.

Second step: The purified Fe_3O_4 NPs were added to 45 mL deionized water. Then, 2.0 mL of TMSPMA was added to the Fe_3O_4 NPs solution under mechanical agitation at room temperature. Surface silanization of Fe_3O_4 MNPs was performed for 24 hours. Then, Surface modified Fe_3O_4 MNPs were gathered and rinsed with deionized water several times by a magnet (Fig. 1).

Third step: TMSPMA-functionalized Fe_3O_4 (2.5 g) and 500 mL of Toluene were added to the 1-L flask and then the mixture was subjected to ultrasound for 10 minutes. After dispersing, 7.0 g of 4-vinylpyridine was monomerically dissolved in the mixture. Then 0.07 g of AIBN was added to the piston and the reaction container was warmed to 70°C for initiating solution polymerization under N_2 atmosphere and agitation for 24 hours. After the polymerization step, the resolution was rinsed once with acetone, and the free P4VP was extracted in Soxhlet apparatus with hot methanol for 36 hours. Finally, P4VP-grafted Fe_3O_4 MNPs were prepared. The formation of functionalized NPs is shown in Fig. 2.

2.2. Batch Sorption Studies

Batch sorption experiments were performed by setting the precise quantity of $\text{Fe}_3\text{O}_4/\text{SiO}_2/\text{P4VP}$ nanosorbent in 25 mL solution under different situations. The primary pH value of the aqueous solution was set with 0.1 M HNO_3 and 0.1 M NaOH or 0.1 M NH_3 . The effect of the most important parameters in different ranges (these ranges were chosen based on similar studies) was investigated as follows:

1. The aqueous solution pH values were varied between 1.5 to 9, at 25°C and time of 210 minutes.



Fig. 1. Adsorbent Appearance Before and After Separation With the Magnetic Field (Magnet).

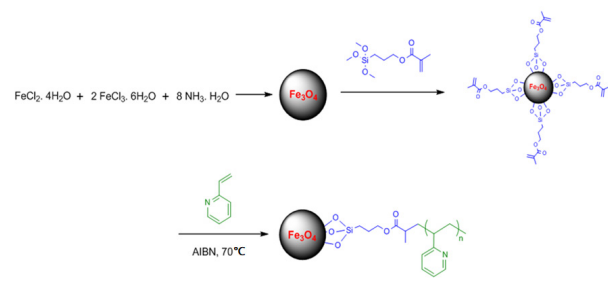


Fig. 2. Schematic of the Synthesis of Functional Fe_3O_4 Nanoparticles.

- The adsorbent dose values were varied between 0.01 and 0.1 g, at a temperature of 25°C, in 210 minutes contact time, and with optimum pH.
- The metal concentrations were varied between 0.5–3 mg/L, at a temperature of 25°C, in 210 minutes contact time, and with optimum pH and adsorbent dose.
- The influence of contact time was examined by changing the time from 5 to 120 minutes, at 25°C and with selected pH value, adsorbent dosage, and initial concentration.
- The impact of temperature was investigated in the range of 20–40°C, in 210 minutes, and with an optimum pH, adsorbent dose and initial concentration.

The percentage of removal efficiency (1), desorption (2) and the adsorption capacity (3) for Mo(VI) ions were determined based on the following formulas:

$$\text{removal efficiency \%} = \frac{C_0 - C_e}{C_0} \times 100 \quad (1)$$

$$\text{desorption \%} = \frac{m_d}{m_a} \times 100 \quad (2)$$

$$\text{sorption capacity } (q_e) = (C_0 - C_e) \times \frac{V}{m} \quad (3)$$

Where C_0 and C_e (mg/L) are the initial and equilibrium liquid-phase concentrations of metal ions, respectively. The value q_e (mg/g) is the sorption capacity. Values m_d and m_a are the desorption and adsorption of ions from the adsorbent surface (mg), respectively. V (L) is the volume of the solution and m (g) is the weight of dried used adsorbent.

3. Results and Discussion

3.1. Adsorbent Characterization

3.1.2. FT-IR Spectroscopy

To ascertain the presence of SiO_2 and P4VP on Fe_3O_4 MNPs, FTIR spectra were provided from Fe_3O_4 MNPs, $\text{Fe}_3\text{O}_4/\text{SiO}_2$, and $\text{Fe}_3\text{O}_4/\text{SiO}_2/\text{P4VP}$ (Fig. 3). From the FTIR spectra shown in Fig. 3 (curve a), it is evident that the characteristic peak of Fe_3O_4 MNPs appeared at 588 cm^{-1} . This band was shifted to a high wave number compared to the Fe-O bond peak of bulk magnetite at 570 cm^{-1} due to nanoparticle size (38). The Si-O-Si bond's asymmetric stretching vibration at 1100 cm^{-1} and symmetric stretching vibration at around 800 cm^{-1} appear in $\text{Fe}_3\text{O}_4/\text{SiO}_2$ and $\text{Fe}_3\text{O}_4/\text{SiO}_2/\text{P4VP}$ spectra (Fig. 3 (curve b and c)), which indicates that the silica has successfully coated on the surface of Fe_3O_4 NPs.

Moreover, the peaks around 1583 , 1463 , and 1367 cm^{-1} which occurred in $\text{Fe}_3\text{O}_4/\text{SiO}_2/\text{P4VP}$ spectra, could be

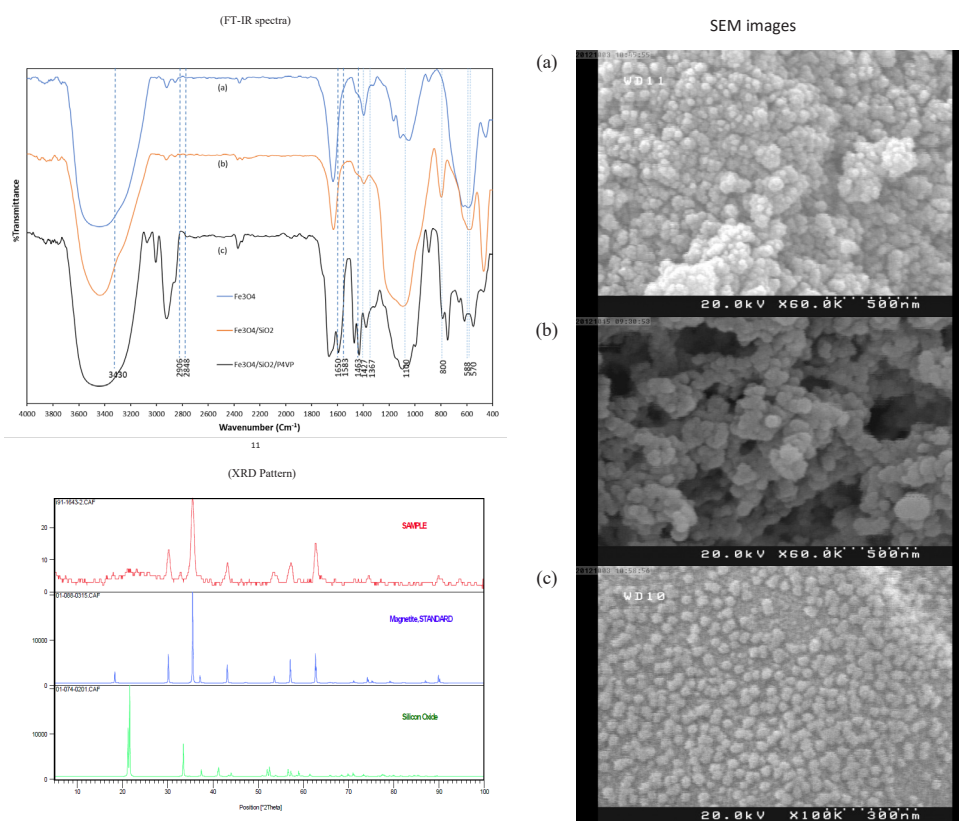


Fig. 3. FT-IR Spectra of Fe_3O_4 , $\text{Fe}_3\text{O}_4/\text{SiO}_2$, and $\text{Fe}_3\text{O}_4/\text{SiO}_2/\text{P4VP}$, XRD Pattern of Fe_3O_4 Nanoparticles, SiO_2 and $\text{Fe}_3\text{O}_4/\text{SiO}_2$, and SEM Images of (a) Base Magnetite Particles, (b) $\text{Fe}_3\text{O}_4/\text{SiO}_2$ Particles and (c) $\text{Fe}_3\text{O}_4/\text{SiO}_2/\text{P4VP}$ Particles

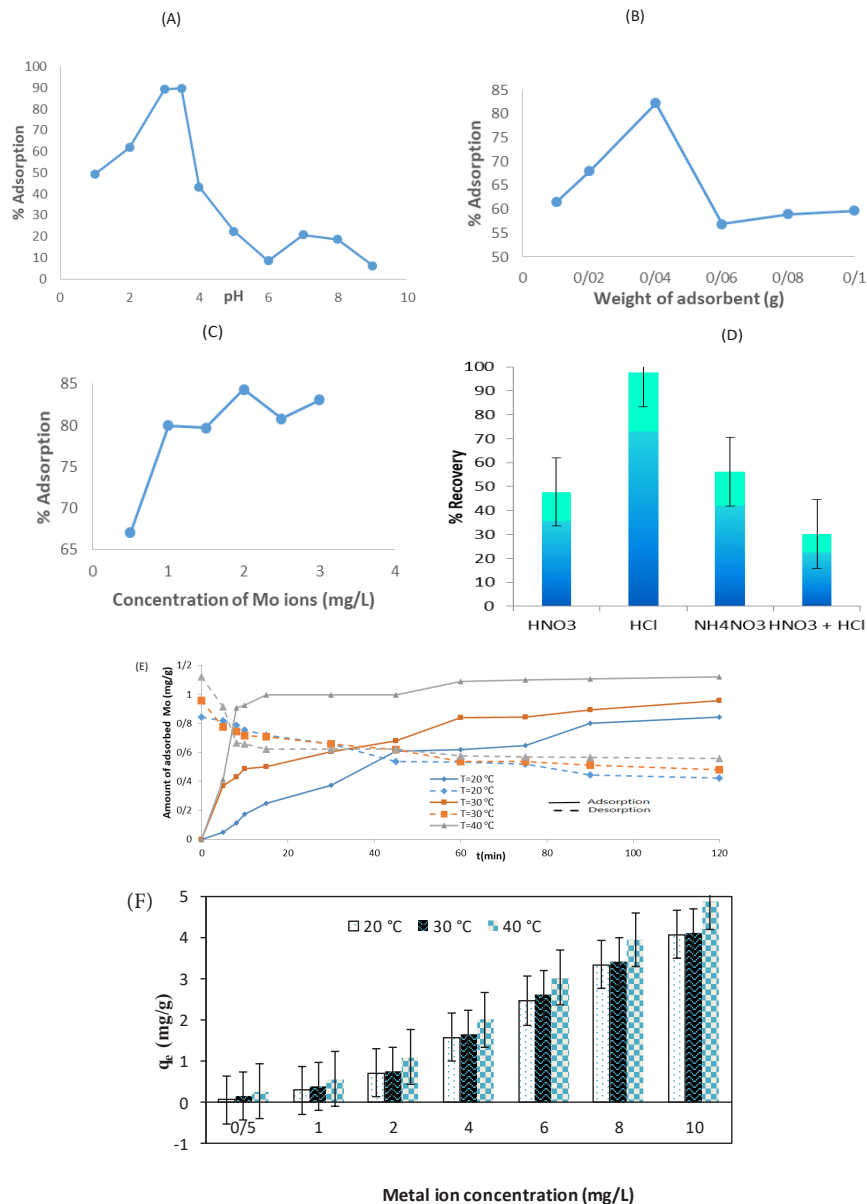


Fig. 4. (A) Effect of pH, (B) Sorbent Dosage, and (C) Initial Concentration of Mo(VI) on the Sorption of Mo(VI) Ions by Adsorbent, (D) Desorption Results of Mo(VI) from Adsorbent Surface at Different Solvents, (E) Effect of Contact time at Different Temperatures on the Adsorption and Desorption Processes, (F) Effect of Temperature on the Adsorption of Mo(VI) Onto the Adsorbent.

assigned as features of pyridine cycle and amine in the P4VP molecules. The absorption bands at about 3430 and 1650 cm^{-1} in all the spectra mainly originate from the -OH vibrations in H_2O . Based on the presence of bands in the range of 2848–2906 cm^{-1} and 1427 cm^{-1} , which correspond to the -CH_2 stretching vibration in P4VP / Fe_3O_4 / SiO_2 FTIR spectrum (black line in FTIR spectra), one can deduce that the P4VP molecules are bonded to the surface of Fe_3O_4 / SiO_2 .

3.1.3. XRD Pattern

Fig. 1 shows the X-ray diffraction result of the base

magnetite particles. The result revealed diffraction peaks at $2\theta = 30.13, 35.54, 43.11, 53.73, 57.30$ and 62.77 , which are characteristic peaks of magnetite (Fe_3O_4) crystals (39). The average diameter which can be evaluated from the Scherrer equation ($D = 0.9\lambda / \beta \cos\theta$, where D is the average diameter, λ is the x-ray wavelength, β is the full width at wide half maximum and θ is the x-ray diffraction angel), is 42.4 nm. The XRD pattern of $\text{Fe}_3\text{O}_4/\text{SiO}_2$ NPs (Fig. 3) revealed that the binding and TMSPPMA did not cause any measurable change in the phase property of Fe_3O_4 cores. This could be attributed to the fact that the binding and TMSPPMA occurred only on the surface of

the Fe_3O_4 cores to form a core-shell structure.

3.1.4. Scanning Electron Microscopy

For obtaining more direct information on particle size and morphology, the SEM micrograph of base magnetite particles, $\text{Fe}_3\text{O}_4/\text{SiO}_2$ and $\text{Fe}_3\text{O}_4/\text{SiO}_2/\text{P4VP}$ were provided. SEM photographs showed that the silanized MNPs (Fig. 3b) were roughly spherical in shape, and the average size of these particles was very close to the average size of base magnetite particles (Fig. 3a). The size distribution was 35.1–40.6 nm in base magnetite particles which almost matches the calculated value by the Scherrer equation. Fig. 3b, c represents the SEM images of $\text{Fe}_3\text{O}_4/\text{SiO}_2$ and $\text{Fe}_3\text{O}_4/\text{SiO}_2/\text{P4VP}$. The morphology and size almost maintained the original state (32.8 and 36 nm, respectively).

3.2. Adsorption Investigations

3.2.1. Effect of pH

The pH of the solution is an essential agent that has a great impact on the adsorption of metal ions. This is strikingly due to the difference in chemical characteristics of the sorbent, sorbate, and the ionization of dissolved ions, which can change the kinetic and equilibrium properties of the sorption process (40). Batch sorption experiments of Mo(VI) were performed by putting 0.01 g of $\text{Fe}_3\text{O}_4/\text{SiO}_2/\text{P4VP}$ nanosorbent in 25 mL of the metal solutions (2 mg/L) for 210 minutes. The pH value of the solutions was regulated with 0.1 M HNO_3 or 0.1 M NaOH. The pH value was evaluated in the range of 1.5 to 9. The adsorption efficiency of Mo(VI) on the adsorbent as the purpose of initial solution pH (1.5–9) is shown in Fig. 4A. At a pH value of 2.5 and minor quantities, there was a powerful condition to develop a chelate complex with the amine combinations of the sorbent between H^+ and Mo (VI) ions. This was due to the condition in which by reducing the pH, the protonation percentage of the amine combinations increased and, conversely, the number of active sorption sites for the metal ions adsorption decreased. By increasing the pH from 2.5 to 3.5, the positive charge density of the sorption reduced (due to the decrement in H^+ concentration), and the active positions of the sorbent easily absorbed the metal ions. The adsorption efficiency for Mo(VI) was obtained with 89.8% (at pH=3.5). At pH values above 3.5, the metal ions precipitated out as metal hydroxide due to the high concentration of OH anions. Therefore, the optimal pH range of 3.5 was chosen.

3.2.2. Effect of Adsorbent Dose

The effect of the adsorbent dose on the amount of Mo (VI) sorption is shown in Fig. 4B. The sorption of Mo(VI) by the synthesized material ($\text{Fe}_3\text{O}_4/\text{SiO}_2/\text{P4VP}$) was examined by changing the mass of sorbent in solutions, while keeping other parameters constant. By increasing the sorbent amount from 0.01 to 0.04 g, the adsorption efficiency was increased from 61.5 to 82.3%; but by re-

rising it from 0.04 to 0.1 g, the adsorption efficiency was decreased. By increasing the sorption dose with a uniform metal ion concentration, the sorption sites are not saturated completely. At higher ratios of the mass of the adsorbent to concentration of metal ions, there was a surface sorption causing the metal ion concentration to decrease again when the ratio was reduced. This phenomenon is because of the fact that a specific quantity of sorbate can be separated by a solid enrichment of the adsorbent. The metal ions adsorbed causes a decrease in dose of the sorbent, which is due to a decrease in the concentration gradient between the concentrations of metal ions in the solution and on the surface of the sorbent. In addition, this reduction can be attributed to a partial covering or aggregation of sorption sites, which leads to a reduction in the total accessible sorbent surface for the metal ions and to an extension of the path of propagation (41,42). Finally, the best adsorbent dose was determined to be 0.04 g.

3.2.3. Effect of Initial Concentration

The effect of initial concentration (C_0) on the adsorption characteristics was intensively investigated for $\text{Fe}_3\text{O}_4/\text{SiO}_2/\text{P4VP}$ by varying C_0 of Mo(VI) from 0.5 to 3 mg/L at 25°C. The remaining conditions stayed fixed (no change) over the course of the tests. The results are shown in Fig. 4C. Under optimum conditions, the adsorption efficiency of Mo(VI) increased with the expansion of the initial Mo(VI) concentration from 67% to 83.1%. The phenomenon can be attributed to the fact that the total available adsorption sites are not entirely filled with a fixed adsorbent dose, which leads to an enrichment of the adsorption percentage of adsorbate. Eventually, 2 mg/L was selected as optimum C_0 to continue the experiments.

3.2.4. Desorption Study

Four aqueous solutions (each 25 mL) containing Mo(VI) ions (2 mg/L) were magnetically stirred with 0.04 g of the $\text{Fe}_3\text{O}_4/\text{SiO}_2/\text{P4VP}$ particles, at 25°C and for 210 minutes. The uptake amount was 84.5% for Mo(VI) ions. The loaded adsorbents were filtered-off and then were contacted with 10 mL of HNO_3 , HCl, NH_4NO_3 , and a mixture of HNO_3 and HCl (1 M), separately. It was observed that the adsorbed ions were desorbed quantitatively using HCl (Fig. 4D). Then, to determine the optimal concentration of HCl, the used adsorbent was transferred to 10 mL of HCl in the concentration area of 0.5–5 M. The concentration of Mo(VI) was evaluated as previously mentioned. The desorption course was also followed to extract Mo(VI) ions from wastewater and adsorbent. According to the results shown in Table 1, HCl 1 M Mo(VI) is suitable for recovery.

3.2.5. Effect of Contact Time and Temperature

The variations of Mo(VI) sorption amount in relation to the contact time in various temperatures (20, 30 and

40°C) were investigated (Fig. 4E). The other parameters stayed constant during the experiments. As it can be stated, the sorption of the Mo(VI) ions occurs in two stages: the first stage involves an external diffusion that follows the introduction of the metal ions into the outer surface of the adsorbent, which is a quick step (rapid phase). The second stage comprises a pore diffusion which follows the sorption of the metal ions on the inner surface of the adsorbent (drag phase). It was evident that the amount of Mo(VI) adsorbed was increased by an increase in the temperature. For Mo ions, the sorption rate was immediate within the first minutes (10 minutes), and this rate gradually decreased as it reached equilibrium. It was concluded that the sorption of Mo(VI) species onto the $\text{Fe}_3\text{O}_4/\text{SiO}_2/\text{P4VP}$ sorbent was an endothermic process. Ultimately, sorption is inherently exothermic and diffusion is an endothermic process. With an increase in the amount of adsorption due to rising temperatures, it was concluded that the role of the diffusion process had been more significant than the sorption progress. Under corresponding initial Mo(VI) concentrations from 0.5 to 10 mg/L, the adsorption capacity of Mo(VI) increased with an increase in temperature from 20 to 40°C. The temperature effect on the sorption capacity at the equilibrium state is demonstrated in the Table 2 and Fig. 4F.

Table 1. Desorption Results of Mo(VI) from $\text{Fe}_3\text{O}_4/\text{SiO}_2/\text{P4VP}$ Surface With HCl as Stripping Agent at Different Concentrations

HCl Concentration (M)	Recovery (%)
0.5	45.65
1	98.0
2	53.0
3	45.45
4	58.35
5	47.85

3.2.6. Sorption Kinetics

Kinetics of the adsorption process is extremely important and remarkable for modeling and designing the sorption developed in the industries, as well as for describing the adsorption rate of dissolved substances, and it determines the time required for the adsorption reaction. Therefore, the kinetics of the removal of Mo(VI) ions was determined in this study in order for determining the sorption behavior of $\text{Fe}_3\text{O}_4/\text{SiO}_2/\text{P4VP}$. Various kinetic models were considered to describe the experimental data obtained from the experiments, and to clarify the development of the kinetic sorption (Table 3). The pseudo-first order, pseudo-second order, and intraparticle diffusion types were all analyzed to describe the kinetic data obtained from the experiments. The parameters including rate constants (k_1 , k_2) and correlation coefficients were computed; the calculated parameters are shown in Table 4 and Fig. 5. The correlation coefficient values of the pseudo-first-order model were lower than the pseudo-second-order model. As can be seen in Table 4 below, the pseudo-second order model belongs to the kinetic data and describes the data more consistently due to the high value of the correlation coefficient ($R^2 > 0.99$). The temperature effect on the adsorption rate constant was determined using the Arrhenius-type relationship (Table 3). The k_0 of E_a were 7.9×10^{12} g/mg.min and 82.5497 kJ/mol with a C_0 of 2.0 mg/L. The magnitude of activation energy showed a type of adsorption that was physical or chemical. Achieving activation energy of 5–40 kJ/mol coincides with physisorption mechanism, while achieving activation energy of 40–800 kJ/mol coincides with chemisorption mechanism(32). The activation energy (E_a) in this study was 82.5497 kJ/mol, which is associated with chemisorption and has a higher potential.

3.2.7. Adsorption Isotherms and Thermodynamic Properties

Adsorption isotherm data obtained from the experiments were examined by the Generalized, Fritz

Table 2. Equilibrium Results With Mo(VI) Ions Initial Concentrations From 0.5 to 10 mg/L and Temperatures 293, 303 and 313 k

C_0 (mg/L)	T (K)								
	293			303			313		
	C_e (mg/L)	Kd	q (mg/g)	C_e (mg/L)	Kd	q (mg/g)	C_e (mg/L)	Kd	q (mg/g)
0.5	0.404	0.216	0.06	0.261	1.110	0.149	0.075	5.130	0.266
1	0.541	0.702	0.287	0.400	2.222	0.375	0.111	6.538	0.556
2	0.853	1.075	0.717	0.783	2.467	0.760	0.256	5.366	1.090
4	1.120	2.162	1.800	1.374	2.735	1.641	0.784	3.409	2.010
6	1.412	2.784	2.866	1.828	3.142	2.608	1.165	3.519	3.022
8	1.701	3.114	3.937	2.520	3.111	3.425	1.688	3.108	3.945
10	2.369	2.654	4.769	3.510	2.761	4.056	2.210	2.866	4.869

Table 3. Isotherms, Kinetics, and Other Equations Used in This Study

Models / Equations	Parameters
Generalized model	
$q_e = \frac{q_m C_e^{ng}}{K_g + C_e^{ng}}$	q_e (mg/ g): equilibrium adsorption capacity q_m (mg/ g): maximum adsorption capacity C_e (mg/ L): equilibrium adsorbate concentration in solution ng: generalized equation exponent K_g (mg/ L): generalized constant
Fritz Schlunder model	
$q_e = \frac{K_{f1} C_e^{nf}}{1 + K_{f2} C_e^{mf}}$	K_{f1} (mg/g)(mg/L) nf: fritz schlunder constant K_{f2} (mg/ L) mf : Fritz Schlunder constant nf: fritz schlunder equation exponent mf: fritz schlunder equation exponent
Weber Van Vliet model	
$C_e = K_w q_e^{(nwq_e^{mw} + lw)}$	K_w : weber van vliet constant nw: weber van vliet equation exponent mw: weber van vliet equation exponent lw: weber van vliet equation exponent
Pseudo-first-order kinetic model	
$\ln(q_e - q_t) = \ln q_e - k_1 t$	q_t (mg/L): amount of adsorbate adsorbed at time t k_1 (min ⁻¹): pseudo-first-order rate constant
Pseudo- second order kinetic model	
$\frac{t}{q_t} = \frac{1}{k_2 q_e^2} + \frac{t}{q_e}$	k_2 (g mg.min ⁻¹): pseudo-second-order rate constant t (min): time
Intraparticle diffusion model	
$q_t = k_p t^{1/2} + C_t$	k_p (mg/g.min ^{1/2}): intraparticle diffusion rate constant
Arrhenius equation	
$k = k_0 e^{-E_a/RT}$	k_0 : Arrhenius constant E_a (kJ /mol):activation energy
Clausius-Clapeyron equations	
$\frac{d(\ln C_e)}{dT} = -\frac{\Delta H_x}{RT^2}$	ΔH_x (kJ /mol): isosteric heat of adsorption ΔH^* (kJ /mol): activation enthalpy change ΔS^* (kJ/ mol.K): activation entropy change ΔG^* (kJ /mol): activation Gibbs energy change k_B : Boltzmann constant
$\ln\left(\frac{k}{T}\right) = \ln\left(\frac{k_B}{h_p}\right) + \frac{\Delta S^*}{R} - \frac{\Delta H^*}{RT}$	K_e : equilibrium constant ΔH^* (kJ /mol): standard enthalpy change ΔS^* (kJ /mol.K): standard entropy change
$\Delta G^* = \Delta H^* - T\Delta S^*$	
$\ln(K_e) = -\frac{\Delta H^0}{RT} + \frac{\Delta S^0}{R}$	ΔG^* (kJ /mol): standard Gibbs free energy change C_0 (mg/ L): initial adsorbate concentration in solution
$K_e = \frac{C_0 - C_e}{C_e}$	
$\Delta G^0 = \Delta H^0 - T\Delta S^0$	
Error equations	
$RMSE = \sqrt{\frac{\sum_{i=1}^n (x_{obs,i} - x_{model,i})^2}{n}}$	
$\chi^2 = \frac{\sum_{i=1}^n (x_{obs,i} - x_{model,i})^2}{x_{model,i}}$	

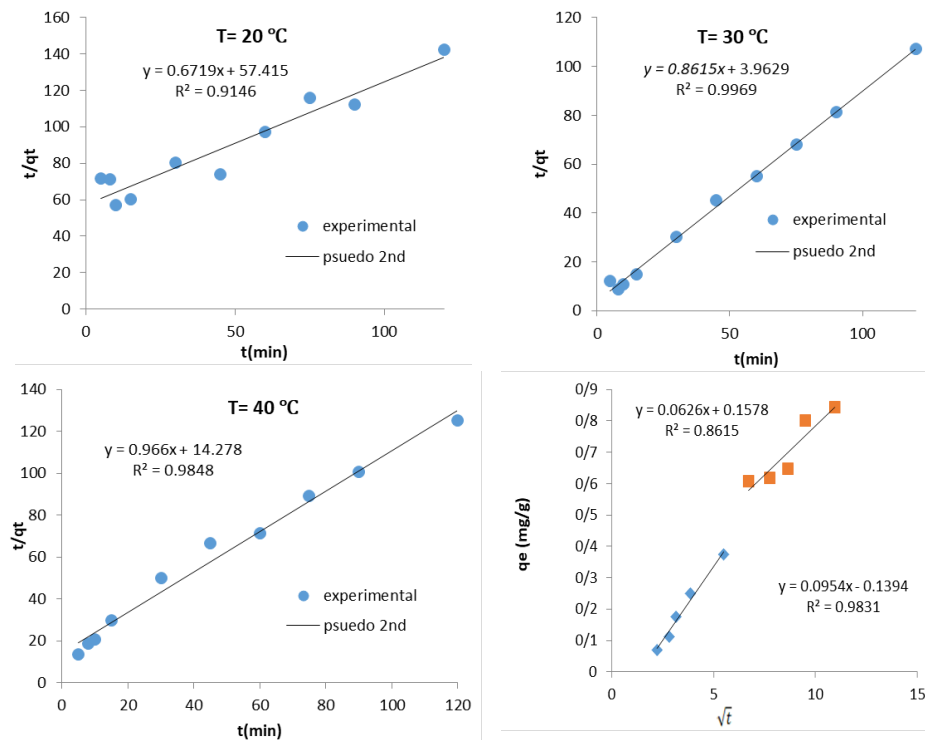


Fig. 5. Pseudo-Second-Order Plots and Webber Morris Model for the Mo(VI) Ions Removal Onto the Adsorbent.

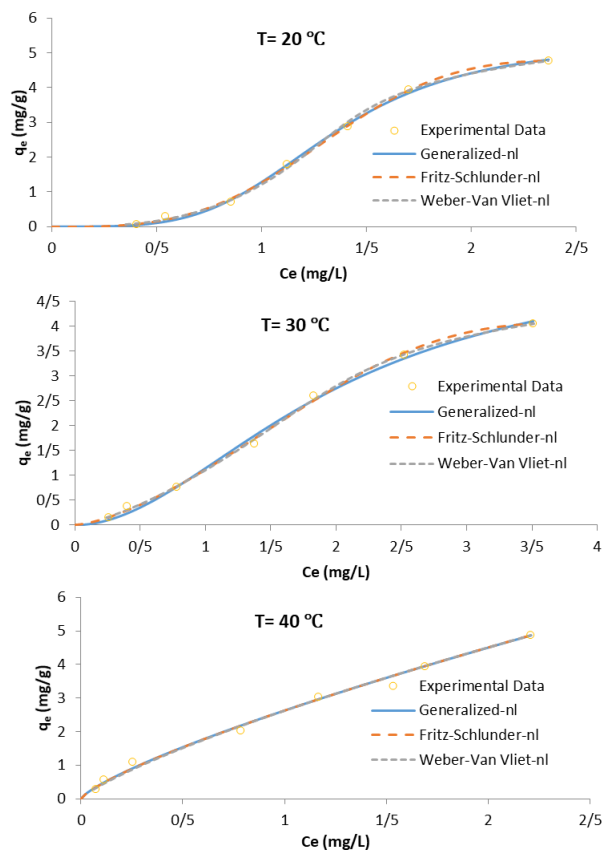


Fig. 6. Isotherm Curves Obtained by the Best Non-Linear Modeling at Different Temperatures.

Schlunder and Weber Van Vliet isotherm models. The forms can be explained by equations (see Table 3). The three models adsorption isotherms are presented in Table 5 and the curves are presented in Fig. 6.

The adsorption of Mo(IV) onto Fe₃O₄/SiO₂/P4VP at different temperatures showed (Fig. 4F and Table 4) an ascent in the adsorption amount with rising temperatures. The standard Gibbs free energy change (ΔG°) is the basic principle of spontaneity. Reactions are spontaneous at a certain temperature when ΔG° has a negative value. The standard enthalpy change (ΔH°), standard entropy change (ΔS°) and standard Gibbs free energy change (ΔG°), which were associated with the adsorption course, were calculated using the equations (see Table 3). The plot of $\ln K_d$ vs. $1/T$ for the adsorption of Mo (VI) was drawn, which presented the values of ΔH° and ΔS° obtained from the slope and intercept, respectively. The ΔG° was also calculated based on ΔH° and ΔS° (see Table 3). The value of the obtained parameters was shown in Table 6. The ΔH° and ΔS° were found to be 61.30 kJ/mol and 209.84 J/mol K, respectively. The positive results of ΔH° suggested the endothermic nature of adsorption of the Mo(VI) ions on Fe₃O₄/SiO₂/P4VP.

The positive ΔS° results showed the growing possibility at the interface between solid and solution during the adsorption course. The positive ΔS° of adsorption also represented the affinity of the adsorbent for the Mo(VI)

Table 4. Parameters for Kinetic Models of Mo (VI) Sorption Onto Fe₃O₄/SiO₂/P4VP

T(K)	q _{e,exp} (mg/ g)	Pseudo First Order Kinetic Model				
		q _{e,cal} (mg/ g)	k ₁ (min ⁻¹)	R ²	Δq%	
293	0.8425	0.9265	0.0279	0.9059	9.97	
303	1.1187	0.4865	0.0423	0.8724	56.51	
313	0.9575	0.7283	0.0265	0.9602	23.93	
T(K)	q _{e,exp} (mg/ g)	Pseudo Second Order Kinetic Model				
		q _{e,cal} (mg/ g)	k ₂ (g/ mg.min)	R ²	Δq%	
293	0.8425	1.4883	0.0079	0.9146	76.65	
303	1.1187	1.1608	0.1873	0.9969	3.76	
313	0.9575	1.0352	0.0654	0.9848	8.11	
T(K)	q _{e,exp} (mg/ g)	Intraparticle Diffusion Model				
		q _{e,cal} (mg/ g)	K _p (g/ mg.min)	C _i (mg/ g)	R ²	Δq%
293	0.8425	0.8454	0.07717	1.81×10 ⁻⁶	0.9516	0.34
303	1.1187	1.5095	0.1378	0.4293	0.1956	34.93
313	0.9575	1.1042	1.1042	0.1558	0.8571	15.32

Solution Volume=25 mL; Initial Mo(VI) concentrations =2 mg/L; Sorbent Dosage=0.04g; pH=3.5.

Table 5. Generalized, Fritz Schlunder, and Weber Van Vliet Isotherm Constants for the Adsorption of Mo(VI) Ions Onto Fe₃O₄/SiO₂/P4VP

T(K)	Generalized Model						
	q _m	k	n	R ²	RMSE	χ ²	
293	5.2856	3.1218	3.9821	0.9979	0.0777	0.0014	
303	5.4652	3.7745	1.9390	0.9956	0.0944	0.0025	
313	2.7503×10 ¹⁵	1.0461×10 ¹⁵	0.7766	0.9959	0.1046	0.0021	
T(K)	Fritz Schlunder Model						
	K ₁	K ₂	n	m	R ²	RMSE	χ ²
293	1.4012	0.1013	3.1126	4.0401	0.9988	0.0596	0.0005
303	1.1307	0.0152	1.4746	3.1363	0.9979	0.0646	0.0014
313	8.0934	2.0782	0.7766	1.8276×10 ⁻⁸	0.9959	0.1046	0.0021
T(K)	Weber Van Vliet Model						
	k	n	m	l	R ²	RMSE	χ ²
293	0.9343	8.3131×10 ⁻⁵	5.1146	0.3498	0.9967	0.0370	0.0005
303	0.9291	1.1208×10 ⁻⁴	5.4726	0.7112	0.9989	0.0372	0.0004
313	0.3042	-18.4924	-0.0013	19.7058	0.9972	0.0446	0.0007

Table 6. Thermodynamic Results of Mo(VI) Ions Adsorption by Fe₃O₄/SiO₂/P4VP in Temperatures of 293, 303 and 313

Temperature (K)	ΔG° (kJ/ mol)	ΔH° (kJ/ mol)	ΔS°(J/ mol.K)
293	-0.177	61.30	209.84
303	-2.276		
313	-0.374		

Table 7. Comparison Between the Results of This Study and Some Similar Studies

Adsorbent	Optimal pH	Capacity (mg/g)	Best Fitted Isotherm Model	Equilibrium Time (min)	Best Fitted Kinetic Model	Reference
Fe ₃ O ₄ /SiO ₂ /P4VP	3.5	4.87	Weber Van Vliet	210	Pseudo-second-order	Present study
Modified resin with aniline formaldehyde	5	3.1 4.03	Freundlich	5	-	(41)
Di-(2-ethylhexyl) phosphoric acid coated silanized magnetite nanoparticles	-	25.84	Langmuir	-	-	(42)
Macroporous resin	7.25	228.2	Freundlich	25	-	(43)
Nanometer-sized titanium dioxide	1	2.01				(44)

ion. Negative values of ΔG° for Mo(VI) adsorption by $\text{Fe}_3\text{O}_4/\text{SiO}_2/\text{P4VP}$ indicated that the adsorption process was spontaneous and feasible. Table 7 compares the results of this study with several similar works.

3.2.8. Effect of Foreign Ions

To judge the separation of the preconcentration system, the performance of several metal ions (5 mg/L) was investigated for the sorption behavior of Mo(VI) ions (5 mg/L). The results were displayed in Table 8. This table shows that the best competitive ions in adsorption of Mo(VI) ions onto $\text{Fe}_3\text{O}_4/\text{SiO}_2/\text{P4VP}$, were Co(II) and Pt(IV). The significance of other foreign ions mentioned at certain concentrations was marginal. The adsorption of Mo(VI) ions on $\text{Fe}_3\text{O}_4/\text{SiO}_2/\text{P4VP}$ in the presence of all mentioned ions (solution volume=25 mL, adsorbent amount=0.04 g, concentration of each ion=5 mg/L) was evaluated. The Mo(VI) ions in the environmental samples can be made available quantitatively.

3.2.9. Application of Method

The $\text{Fe}_3\text{O}_4/\text{SiO}_2/\text{P4VP}$ was used to preconcentrate and determine Mo(VI) ions in two real samples (Tehran tap water and spring water). The pH of the water samples

Table 8. Effect of Interfering Ions on Sorption

Interfering Ion	A (mg/L)	%E	%L	D
-	4.75	95.04	0	59.40
Cd ²⁺	4.47	89.40	5.89	55.88
Ni ²⁺	4.32	86.40	9.05	54.00
Ca ²⁺	4.43	88.52	6.74	55.32
Co ²⁺	4.14	84.50	12.84	52.81
Fe ³⁺	4.46	89.40	6.10	55.88
Ba ²⁺	4.51	90.12	5.05	56.32
Pt ⁴⁺	4.17	83.30	12.21	52.06
Mixed Above	4.15	83.00	12.63	51.88

A: Amount of adsorbed Mo(VI), $L=(C_e^{\text{No-ion}}-C_e)/C_e^{\text{No-ion}}$; Loss adsorption (%), $E=(C_0-C_e)/C_0$; Extraction percentage (%), and $D=Q/C_e$; distribution ratio

was adjusted to 3.5. After detecting Mo(VI) ions in the samples, the amounts of 0.2, 0.4 and 0.6 mg/L of Mo(VI) ions were added to 25 mL of these samples and mixed with 0.04 g of adsorbent and stirred for 3.5 hours. The obtained results are presented in Table 9. These results show the practical applicability for the Mo(VI) determination in samples.

4. Conclusion

In this study, the adsorption isotherms, kinetic, and thermodynamic properties related to adsorption of Mo(VI) ions on $\text{Fe}_3\text{O}_4/\text{SiO}_2/\text{P4VP}$ were analyzed using batch-adsorption techniques. The magnetic P4VP was prepared by copolymerization of P4VP with TMSMA. Several techniques such as FTIR, SEM, and XRD were used for the characterization of the prepared adsorbent. The optimum conditions were determined for Mo(VI) ions adsorption. The values of parameters in tests were: pH (3.5), adsorbent dose (0.04 g), initial Mo(VI) ions concentration (2.0 mg/L), contact time range (0 to 120 minutes), and temperatures (20, 30 and 40°C). In desorption studies, it was found that the 1M HCl was suitable for Mo(IV) ions recovery. The adsorption of Mo(VI) ions on $\text{Fe}_3\text{O}_4/\text{SiO}_2/\text{P4VP}$ tends to Kinetics of adsorption with high correlation Pseudo-kinetics of second order. The E_a value of 82.5497 kJ/mol reported in this study indicated that the adsorption had a higher potential in the context of chemisorption and because of the negative ΔG° and the positive ΔH° , the total adsorption course was endothermic and spontaneous. The equilibrium data were analyzed with Generalized, Fritz Schlunder and Weber Van Vliet isotherm models. The information gained from our investigation provided excellent results for the Fritz Schlunder model compared to other models. We determined the influence of other ions including Cd²⁺, Ca²⁺, Co²⁺, Fe³⁺, Ba²⁺, and Pt⁴⁺ on the uptake of Mo(IV) ions. The results showed that the most effective ions in the uptake of Mo(IV) ions on $\text{Fe}_3\text{O}_4/\text{SiO}_2/\text{P4VP}$ were Co(II) and Pt(IV), while the effect of other foreign ions, which were inserted at certain concentrations, was found to be minor. The uptake

Table 9. Results Obtained for Mo(VI) Ion Determination in Real Samples

Water Samples	Found Mo(VI) (Without Spiking) (mg/L)	Added Mo(VI) (mg/L)	Found Mo(VI) Average (After Spiking) (mg/L)	Pre-concentration Factor	Recovery (%)	SD	Relative SD (%) ^a
Tap water	ND	0.2	0.25	10	123.4	0.321	13.03
		0.4	0.40	10	100.8	0.153	3.79
		0.6	0.61	10	102.2	0.306	4.98
Spring water	0.12	0.2	0.27	10	83.3	0.153	5.73
		0.4	0.42	10	80.1	0.153	3.67
		0.6	0.72	10	99.5	0.208	2.90

ND: Not Detected; SD, standard deviation.

a, for three determinations

of Mo(VI) ions on $\text{Fe}_3\text{O}_4/\text{SiO}_2/\text{P4VP}$ in the presence of all above-mentioned ions (solution volume=25 mL, adsorbent amount=0.04 g, concentration of each ion=5 mg/L) showed that the amount of Mo(VI) ions is measurable in the environmental samples.

Conflict of Interest Disclosures

The authors declare that they have no competing interests.

Acknowledgements

The authors would like to express their heartfelt thanks to all those who aided them with conducting this study, as well as to the nuclear science and technology research institute for financial and technical supports.

References

1. El-Moselhy MM, Sengupta AK, Smith R. Carminic acid modified anion exchanger for the removal and preconcentration of Mo(VI) from wastewater. *J Hazard Mater*. 2011;185(1):442-6. doi: [10.1016/j.jhazmat.2010.09.052](https://doi.org/10.1016/j.jhazmat.2010.09.052).
2. Arthur D. Interrelationships of molybdenum and copper in the diet of the guinea pig. *J Nutr*. 1965;87(1):69-76. doi: [10.1093/jn/87.1.69](https://doi.org/10.1093/jn/87.1.69).
3. Shan W, Fang D, Zhao Z, Shuang Y, Ning L, Xing Z, et al. Application of orange peel for adsorption separation of molybdenum(VI) from Re-containing industrial effluent. *Biomass Bioenergy*. 2012;37:289-97. doi: [10.1016/j.biombioe.2011.11.015](https://doi.org/10.1016/j.biombioe.2011.11.015).
4. Atia AA, Donia AM, Awed HA. Synthesis of magnetic chelating resins functionalized with tetraethylenepentamine for adsorption of molybdate anions from aqueous solutions. *J Hazard Mater*. 2008;155(1-2):100-8. doi: [10.1016/j.jhazmat.2007.11.035](https://doi.org/10.1016/j.jhazmat.2007.11.035).
5. Pathak SK, Singh SK, Mahtele A, Tripathi SC. Studies on extraction behaviour of molybdenum(VI) from acidic radioactive waste using 2(ethylhexyl) phosphonic acids, mono 2(ethylhexyl) ester (PC-88A)/*n*-dodecane. *J Radioanal Nucl Chem*. 2010;284(3):597-603. doi: [10.1007/s10967-010-0511-y](https://doi.org/10.1007/s10967-010-0511-y).
6. Afkhami A, Conway BE. Investigation of removal of Cr(VI), Mo(VI), W(VI), V(IV), and V(V) oxy-ions from industrial wastewaters by adsorption and electrosorption at high-area carbon cloth. *J Colloid Interface Sci*. 2002;251(2):248-55. doi: [10.1006/jcis.2001.8157](https://doi.org/10.1006/jcis.2001.8157).
7. Afkhami A, Madrakian T, Amini A. Mo(VI) and W(VI) removal from water samples by acid-treated high area carbon cloth. *Desalination*. 2009;243(1):258-64. doi: [10.1016/j.desal.2008.04.028](https://doi.org/10.1016/j.desal.2008.04.028).
8. Wu CH, Lo SL, Lin CF. Competitive adsorption of molybdate, chromate, sulfate, selenate, and selenite on $\gamma\text{-Al}_2\text{O}_3$. *Colloids Surf A Physicochem Eng Asp*. 2000;166(1-3):251-9. doi: [10.1016/S0927-7757\(99\)00404-5](https://doi.org/10.1016/S0927-7757(99)00404-5).
9. Xu N, Christodoulatos C, Braidia W. Adsorption of molybdate and tetrathiomolybdate onto pyrite and goethite: effect of pH and competitive anions. *Chemosphere*. 2006;62(10):1726-35. doi: [10.1016/j.chemosphere.2005.06.025](https://doi.org/10.1016/j.chemosphere.2005.06.025).
10. Bostick BC, Fendorf S, Helz GR. Differential adsorption of molybdate and tetrathiomolybdate on pyrite (FeS_2). *Environ Sci Technol*. 2003;37(2):285-91. doi: [10.1021/es0257467](https://doi.org/10.1021/es0257467).
11. Faghiehian H, Malekpour A, Maragheh MG. Adsorption of molybdate ion by natrolite and clinoptilolite-rich tuffs. *Int J Environ Pollut*. 2002;18(2):181-9. doi: [10.1504/ijep.2002.000704](https://doi.org/10.1504/ijep.2002.000704).
12. Ryden JC, Syers JK, Tillman RW. Inorganic anion sorption and interactions with phosphate sorption by hydrous ferric oxide gel. *J Soil Sci*. 1987;38(2):211-7. doi: [10.1111/j.1365-2389.1987.tb02138.x](https://doi.org/10.1111/j.1365-2389.1987.tb02138.x).
13. Abd Ali ZT, Ismail ZZ. Experimental and modeling study of water defluoridation using waste granular brick in a continuous up-flow fixed bed. *Environ Eng Res*. 2021;26(2):190506. doi: [10.4491/eer.2019.506](https://doi.org/10.4491/eer.2019.506).
14. Griffiths DWL, Hallam HE, Thomas WJ. Infra-red study of adsorption and oxidation of ammonia on silica-supported platinum and silica. *Trans Faraday Soc*. 1968;64(0):3361-9. doi: [10.1039/tf9686403361](https://doi.org/10.1039/tf9686403361).
15. Sun C, Lee JS, Zhang M. Magnetic nanoparticles in MR imaging and drug delivery. *Adv Drug Deliv Rev*. 2008;60(11):1252-65. doi: [10.1016/j.addr.2008.03.018](https://doi.org/10.1016/j.addr.2008.03.018).
16. Laurent S, Forge D, Port M, Roch A, Robic C, Vander Elst L, et al. Magnetic iron oxide nanoparticles: synthesis, stabilization, vectorization, physicochemical characterizations, and biological applications. *Chem Rev*. 2008;108(6):2064-110. doi: [10.1021/cr068445e](https://doi.org/10.1021/cr068445e).
17. Bucak S, Jones DA, Laibinis PE, Hatton TA. Protein separations using colloidal magnetic nanoparticles. *Biotechnol Prog*. 2003;19(2):477-84. doi: [10.1021/bp0200853](https://doi.org/10.1021/bp0200853).
18. White BR, Stackhouse BT, Holcombe JA. Magnetic gamma- Fe_2O_3 nanoparticles coated with poly-L-cysteine for chelation of As(III), Cu(II), Cd(II), Ni(II), Pb(II) and Zn(II). *J Hazard Mater*. 2009;161(2-3):848-53. doi: [10.1016/j.jhazmat.2008.04.105](https://doi.org/10.1016/j.jhazmat.2008.04.105).
19. Savić AB, Čokeša D, Savić Biserčić M, Častvan-Janković I, Petrović R, Živković LS. Multifunctional use of magnetite-coated tuff grains in water treatment: removal of arsenates and phosphates. *Adv Powder Technol*. 2019;30(8):1687-95. doi: [10.1016/j.apt.2019.05.020](https://doi.org/10.1016/j.apt.2019.05.020).
20. Wang Y, Sun D, Liu G, Jiang W. Synthesis of $\text{Fe}_3\text{O}_4@/\text{SiO}_2@/\text{ZnO}$ core-shell structured microspheres and microwave absorption properties. *Adv Powder Technol*. 2015;26(6):1537-43. doi: [10.1016/j.apt.2015.08.014](https://doi.org/10.1016/j.apt.2015.08.014).
21. Hosseini M, Esrafil A, Yegane badi M, Gholami M. New magnetic/Biosilica/Sodium Alginate Composites for removal of Pb(II) ions from aqueous solutions: kinetic and isotherm studies. *J Adv Environ Health Res*. 2018;6(3):160-72. doi: [10.22102/jaehr.2018.126798.1073](https://doi.org/10.22102/jaehr.2018.126798.1073).
22. Zhou L, Wang Y, Liu Z, Huang Q. Characteristics of equilibrium, kinetics studies for adsorption of Hg(II), Cu(II), and Ni(II) ions by thiourea-modified magnetic chitosan microspheres. *J Hazard Mater*. 2009;161(2-3):995-1002. doi: [10.1016/j.jhazmat.2008.04.078](https://doi.org/10.1016/j.jhazmat.2008.04.078).
23. Soto D, Urdaneta J, Pernía K, León O, Muñoz-Bonilla A, Fernández-García M. Heavy metal (Cd^{2+} , Ni^{2+} , Pb^{2+} and Ni^{2+}) adsorption in aqueous solutions by oxidized starches. *Polym Adv Technol*. 2015;26(2):147-52. doi: [10.1002/pat.3439](https://doi.org/10.1002/pat.3439).
24. Hai B, Wu J, Chen X, Protasiewicz JD, Scherson DA. Metal-ion adsorption on carboxyl-bearing self-assembled monolayers covalently bound to magnetic nanoparticles. *Langmuir*. 2005;21(7):3104-5. doi: [10.1021/la0487139](https://doi.org/10.1021/la0487139).
25. Ngomsik AF, Bee A, Draye M, Cote G, Cabuil V. Magnetic nano- and microparticles for metal removal and environmental applications: a review. *C R Chim*. 2005;8(6):963-70. doi: [10.1016/j.crci.2005.01.001](https://doi.org/10.1016/j.crci.2005.01.001).
26. Vilela PB, Dalalibera A, Duminelli EC, Becegato VA, Paulino AT. Adsorption and removal of chromium (VI) contained in aqueous solutions using a chitosan-based hydrogel. *Environ Sci Pollut Res Int*. 2019;26(28):28481-9. doi: [10.1007/s11356-018-3208-3](https://doi.org/10.1007/s11356-018-3208-3).
27. Khosravi M, Azizian S. Synthesis of different nanostructured flower-like iron oxides and study of their performance as

- adsorbent. *Adv Powder Technol.* 2014;25(5):1578-84. doi: [10.1016/j.apt.2014.05.010](https://doi.org/10.1016/j.apt.2014.05.010).
28. Zhu J, Wei S, Chen M, Gu H, Rapole SB, Pallavkar S, et al. Magnetic nanocomposites for environmental remediation. *Adv Powder Technol.* 2013;24(2):459-67. doi: [10.1016/j.apt.2012.10.012](https://doi.org/10.1016/j.apt.2012.10.012).
29. Zou C, Jiang W, Liang J, Sun X, Guan Y. Removal of Pb(II) from aqueous solutions by adsorption on magnetic bentonite. *Environ Sci Pollut Res Int.* 2019;26(2):1315-22. doi: [10.1007/s11356-018-3652-0](https://doi.org/10.1007/s11356-018-3652-0).
30. De Rossi A, Rigon MR, Zapparoli M, Braido RD, Colla LM, Dotto GL, et al. Chromium (VI) biosorption by *Saccharomyces cerevisiae* subjected to chemical and thermal treatments. *Environ Sci Pollut Res Int.* 2018;25(19):19179-86. doi: [10.1007/s11356-018-2377-4](https://doi.org/10.1007/s11356-018-2377-4).
31. Yetimoğlu EK, Fırlak M, Kahraman MV, Deniz S. Removal of Pb²⁺ and Cd²⁺ ions from aqueous solutions using guanidine modified hydrogels. *Polym Adv Technol.* 2011;22(5):612-9. doi: [10.1002/pat.1554](https://doi.org/10.1002/pat.1554).
32. Maddodi SA, Alalwan HA, Alminshid AH, Abbas MN. Isotherm and computational fluid dynamics analysis of nickel ion adsorption from aqueous solution using activated carbon. *S Afr J Chem Eng.* 2020;32:5-12. doi: [10.1016/j.sajce.2020.01.002](https://doi.org/10.1016/j.sajce.2020.01.002).
33. Krueyai Y, Punyapalakul P, Wongrueng A. Removal of haloacetonitrile by adsorption on thiol-functionalized mesoporous composites based on natural rubber and hexagonal mesoporous silica. *Environ Eng Res.* 2015;20(4):342-6. doi: [10.4491/eer.2015.070](https://doi.org/10.4491/eer.2015.070).
34. Tanev PT, Pinnavaia TJ. Mesoporous silica molecular sieves prepared by ionic and neutral surfactant templating: a comparison of physical properties. *Chem Mater.* 1996;8(8):2068-79. doi: [10.1021/cm950549a](https://doi.org/10.1021/cm950549a).
35. Altun T, Ecevit H. Cr(VI) removal using Fe₂O₃-chitosan-cherry kernel shell pyrolytic charcoal composite beads. *Environ Eng Res.* 2020;25(3):426-38. doi: [10.4491/eer.2019.112](https://doi.org/10.4491/eer.2019.112).
36. Baile P, Vidal L, Canals A. A modified zeolite/iron oxide composite as a sorbent for magnetic dispersive solid-phase extraction for the preconcentration of nonsteroidal anti-inflammatory drugs in water and urine samples. *J Chromatogr A.* 2019;1603:33-43. doi: [10.1016/j.chroma.2019.06.039](https://doi.org/10.1016/j.chroma.2019.06.039).
37. Ulusoy Hİ, Yılmaz E, Soylak M. Magnetic solid phase extraction of trace paracetamol and caffeine in synthetic urine and wastewater samples by a using core shell hybrid material consisting of graphene oxide/multiwalled carbon nanotube/Fe₃O₄/SiO₂. *Microchem J.* 2019;145:843-51. doi: [10.1016/j.microc.2018.11.056](https://doi.org/10.1016/j.microc.2018.11.056).
38. Zhai Y, He Q, Han Q, Duan S. Solid-phase extraction of trace metal ions with magnetic nanoparticles modified with 2,6-diaminopyridine. *Microchim Acta.* 2012;178(3-4):405-12. doi: [10.1007/s00604-012-0857-7](https://doi.org/10.1007/s00604-012-0857-7).
39. Chakraborty S, Chowdhury S, Das Saha P. Adsorption of crystal violet from aqueous solution onto NaOH-modified rice husk. *Carbohydr Polym.* 2011;86(4):1533-41. doi: [10.1016/j.carbpol.2011.06.058](https://doi.org/10.1016/j.carbpol.2011.06.058).
40. Walcarius A, Delacôte C. Rate of access to the binding sites in organically modified silicates. 3. Effect of structure and density of functional groups in mesoporous solids obtained by the co-condensation route. *Chem Mater.* 2003;15(22):4181-92. doi: [10.1021/cm031089l](https://doi.org/10.1021/cm031089l).
41. Borowiak-Resterna A, Cierpiszewski R, Prochaska K. Kinetic and equilibrium studies of the removal of cadmium ions from acidic chloride solutions by hydrophobic pyridinecarboxamide extractants. *J Hazard Mater.* 2010;179(1-3):828-33. doi: [10.1016/j.jhazmat.2010.03.078](https://doi.org/10.1016/j.jhazmat.2010.03.078).
42. Mallakpour S, Barati A. Efficient preparation of hybrid nanocomposite coatings based on poly(vinyl alcohol) and silane coupling agent modified TiO₂ nanoparticles. *Prog Org Coat.* 2011;71(4):391-8. doi: [10.1016/j.porgcoat.2011.04.010](https://doi.org/10.1016/j.porgcoat.2011.04.010).
43. Sid Kalal H, Ahmad Panahi H, Framarzi N, Moniri E, Naeemy A, Hoveidi H, et al. New chelating resin for preconcentration and determination of molybdenum by inductive couple plasma atomic emission spectroscopy. *Int J Environ Sci Technol.* 2011;8(3):501-12. doi: [10.1007/bf03326236](https://doi.org/10.1007/bf03326236).
44. Agarwal S, Tyagi I, Gupta VK, Hanifpour F, Maghsudi M, Javadian H. Mo (IV) adsorption from nitric acid media by Di-(2-ethylhexyl) phosphoric acid (D2EHPA) coated silanized magnetite nanoparticles. *J Mol Liq.* 2016;218:346-53. doi: [10.1016/j.molliq.2016.02.057](https://doi.org/10.1016/j.molliq.2016.02.057).